 CMES, vol.4, no.1, pp.85-102, 2003

Indirect RBFN Method with Thin Plate Splines for Numerical Solution of Differential Equations

N. Mai-Duy, T. Tran-Cong[1]

Abstract: This paper reports a mesh-free Indirect Radial Basis Function Network method (IRBFN) using Thin Plate Splines (TPSs) for numerical solution of Differential Equations (DEs) in rectangular and curvilinear coordinates. The adjustable parameters required by the method are the number of centres, their positions and possibly the order of the TPS. The first and second order TPSs which are widely applied in numerical schemes for numerical solution of DEs are employed in this study. The advantage of the TPS over the multiquadric basis function is that the former, with a given order, does not contain the adjustable shape parameter (i.e. the RBF's width) and hence TPS-based RBFN methods require less parametric study. The direct TPS-RBFN method is also considered in some cases for the purpose of comparison with the indirect TPS-RBFN method. The TPS-IRBFN method is verified successfully with a series of problems including linear elliptic PDEs, nonlinear elliptic PDEs, parabolic PDEs and Navier-Stokes equations in rectangular and curvilinear coordinates. Numerical results obtained show that the method achieves the norm of the relative error of the solution of $O(10^{-6})$ for the case of 1D second order DEs using a density of 51, of $O(10^{-7})$ for the case of 2D elliptic PDEs using a density of 20×20 and a Reynolds number $Re = 200$ for the case of Jeffery-Hamel flow with a density of 43×12.

keyword: mesh-free indirect RBFN method, thin plate splines, rectangular coordinates, curvilinear coordinates, Jeffery-Hamel flow, numerical solution, differential equation.

[1] Corresponding author: Telephone +61 7 46312539, Fax +61 7 46 312526, E-mail trancong@usq.edu.au
Faculty of Engineering and Surveying,
University of Southern Queensland, Toowoomba, QLD 4350, Australia

1 Introduction

Neural Networks (NNs) have found applications in many disciplines [Haykin (1999)]. For example, Multilayer Perceptrons (MPs) and Radial Basis Function Networks (RBFNs) have been used in methods for numerical solution of DEs recently [Dissanayake and Phan-Thien (1994); Takeuchi and Kosugi (1994); Kansa (1990); Dubal (1994); Sharan, Kansa and Gupta (1997); Zerroukat, Power and Chen (1998); Zerroukat, Djidjeli and Charafi (2000); Mai-Duy and Tran-Cong (2001a,b,2002)]. The advantages of a NN-based numerical method are its ease of implementation and mesh-free feature. The concept of solving PDEs using NNs was first introduced by Kansa (1990) in the case of RBFNs and by Dissanayake and Phan-Thien (1994) in the case of MP networks. Since then the NN-based methods, especially the ones based on RBFNs, have received a great deal of attention from researchers and achieved significant progress in solving a wide variety of DEs. For example, the MultiQuadric (MQ) RBF approximation schemes were developed successfully for a numerical solution of elliptic PDEs (Laplace, Poisson and biharmonic equations) by Sharan, Kansa and Gupta (1997) and heat transfer problems by Zerroukat, Power and Chen (1998). Atluri has pioneered the truly meshless method based on the local weak form, the Meshless Local Petrov-Galerkin (MLPG) method, and provied a fundamental classification of all the so-called meshless methods [Atluri and Shen (2002a,b)]. Recently, Mai-Duy and Tran-Cong (2001a,b,2002) proposed new point collocation methods based on MQ-RBFNs for approximation of functions and numerical solution of linear ODEs, linear elliptic PDEs and nonlinear Navier-Stokes equations in rectangular coordinates. The so called Direct RBFN (DRBFN) and Indirect RBFN (IRBFN) methods were studied and it was found that the MQ IRBFN method yields a superior accuracy. It should be noted that the accuracy of the MQ RBFN solution is influenced by the value of the shape

parameter (i.e. the RBF's width). A method for determining the optimal value of the shape parameter is yet to be found. There is increasing interest in another RBF in numerical schemes for DEs [Zerroukat, Power and Chen (1998); Zerroukat, Djidjeli and Charafi (2000)], namely the Thin Plate Splines (TPS). The theoretical foundations for this basis function were laid by Duchon (1977). It is interesting that, even with less adjustable parameters, the TPS-based RBFN methods can achieve an accuracy similar to that of the MQ-based method [Zerroukat, Djidjeli and Charafi (2000)]. In this paper, the Indirect RBFN method using TPSs is developed and verified in rectangular and curvilinear coordinates. It should be emphasised here that in this work the employment of numerical integration schemes is introduced in order to deal with the solution of high order DEs and problems in curvilinear coordinates. The paper is organised as follows. The second section presents the numerical formulation of the TPS-IRBFN method for solving DEs in rectangular coordinates and then some test problems governed by linear elliptic PDEs, nonlinear elliptic PDEs and parabolic PDEs are simulated to verify the present method. The third section is to present the implementation of the TPS-IRBFN method in curvilinear coordinates which is verified by the solution of linear Poisson's equation and Navier-Stokes equations. The last section gives some concluding remarks.

2 TPS-IRBFN methods in rectangular coordinates

2.1 Numerical formulation

The basic derivation of the IRBFN method is given elsewhere [Mai-Duy and Tran-Cong (2001a,b,2002)] and further developed here with the use of the Thin Plate Spline given by

$$g^{(i)} = R^{2q}\log(R), \tag{1}$$

where q is the order of the TPS and R is the Euclidean distance between the ith centre $\boldsymbol{c}^{(i)}$ and the collocation point $\boldsymbol{x}$, i.e. $R = \|\boldsymbol{c}^{(i)} - \boldsymbol{x}\|_2$, in which $\boldsymbol{c}, \boldsymbol{x} \in \Re^d$ and d is any positive integer [Schaback (1995); Gutmann (2001); Fornberg, Driscoll, Wright and Charles (2002)]. However, in 2D, TPSs are rigorously justified with extensive theoretical accuracy results and a variational theory as reported by Fornberg, Driscoll, Wright and Charles (2002) who have applied the TPS RBF (1) approximation in a 1D problem. Thus the TPS RBF (1) is applicable in one, two and three dimensions. In the present method the highest order derivatives are expressed in terms of TPS-RBFNs first, followed by successive symbolic integrations to obtain closed form expressions for lower order derivatives and finally the function(s) itself. The general procedure is briefly recaptured as follows. Consider the variable ψ in the governing equation, the function ψ and its derivatives with respect to x_j can be decomposed in terms of basis functions as follows

$$\psi_{,jj}(\boldsymbol{x}) = \sum_{i=1}^{m} w^{(i)} g^{(i)}(\boldsymbol{x}), \tag{2}$$

$$\psi_{,j}(\boldsymbol{x}) = \int \psi_{,jj}(\boldsymbol{x}) dx_j = \sum_{i=1}^{m} w^{(i)} \int g^{(i)}(\boldsymbol{x}) dx_j, \tag{3}$$

$$\psi_j(\boldsymbol{x}) = \int \psi_{,j}(\boldsymbol{x}) dx_j = \sum_{i=1}^{m} w^{(i)} \int \left(\int g^{(i)}(\boldsymbol{x}) dx_j \right) dx_j. \tag{4}$$

where m is the number of centres, $\left\{g^{(i)}\right\}_1^m$ the set of radial basis functions and $\left\{w^{(i)}\right\}_1^m$ the set of RBFN weights. The closed form representations in terms of basis functions thus obtained are then substituted into the governing equations and boundary conditions to "discretise" the system via the mechanism of point collocation at $\left\{\boldsymbol{x}^{(i)}\right\}_1^n$ where n is the number of collocation points [Mai-Duy and Tran-Cong (2001a)]. This process reduces complex systems of differential equations to systems of algebraic equations with the unknown vector being the set of RBFN weights, which can be solved directly by standard numerical algorithms. For the purpose of illustration, let us consider the 2D Poisson's equation over the domain Ω

$$\nabla^2 u = p(\boldsymbol{x}), \qquad \boldsymbol{x} \in \Omega, \tag{5}$$

where ∇^2 is the Laplacian operator, $\boldsymbol{x}$ is the spatial position, p is a known function of $\boldsymbol{x}$ and u is the unknown function of $\boldsymbol{x}$ to be found. Equation (5) is subject to Dirichlet and/or Neumann boundary conditions over the boundary Γ

$$u = p_1(\boldsymbol{x}), \qquad \boldsymbol{x} \in \Gamma_1, \tag{6}$$

$$\boldsymbol{n} \cdot \nabla u = p_2(\boldsymbol{x}), \qquad \boldsymbol{x} \in \Gamma_2, \tag{7}$$

where $\boldsymbol{n}$ is the outward unit normal; ∇ is the gradient operator; Γ_1 and Γ_2 are the boundaries of the domain

such as $\Gamma_1 \cup \Gamma_2 = \Gamma$ and $\Gamma_1 \cap \Gamma_2 = \emptyset$; p_1 and p_2 are known functions of $\boldsymbol{x}$.

The information provided by the given DEs and the associated boundary conditions are taken into account in designing the networks through the following Sum Squared Error (SSE)

$$SSE = \sum_{\boldsymbol{x}^{(i)} \in \Omega} \left[(u_{,11}(\boldsymbol{x}^{(i)}) + u_{,22}(\boldsymbol{x}^{(i)})) - p(\boldsymbol{x}^{(i)}) \right]^2 + \sum_{\boldsymbol{x}^{(i)} \in \Omega} \left[u_1(\boldsymbol{x}^{(i)}) - u_2(\boldsymbol{x}^{(i)}) \right]^2 + \sum_{\boldsymbol{x}^{(i)} \in \Gamma_1} \left[u_1(\boldsymbol{x}^{(i)}) - p_1(\boldsymbol{x}^{(i)}) \right]^2 + \sum_{\boldsymbol{x}^{(i)} \in \Gamma_2} \left[(n_1 u_{,1}(\boldsymbol{x}^{(i)}) + n_2 u_{,2}(\boldsymbol{x}^{(i)})) - p_2(\boldsymbol{x}^{(i)}) \right]^2, \quad (8)$$

where the term $u_1(\boldsymbol{x}^{(i)})$ is symbolically obtained via $u_{,11}$ and $u_2(\boldsymbol{x}^{(i)})$ via $u_{,22}$ in the manner of (2)-(4) above. By substituting the representations for u and its derivatives (2)-(4) into (8), the unknowns in the governing equations are now RBFN weights that are to be found by the process of minimisation. Note that in the present context of solving DEs, the "data" points are more general collocation points instead of just actual given numerical values of the function to be approximated or interpolated. Thus at a data (collocation) point either the DEs (in the case of internal points) or the DEs and the boundary conditions (in the case of boundary points) are forced to satisfy. The *SSE* above can be rewritten in the short form as

$$\min \|\mathbf{A}\boldsymbol{w} - \boldsymbol{y}\|_2, \quad (9)$$

where $\mathbf{A}$ is regarded as the design matrix, $\boldsymbol{y}$ is a known vector and $\boldsymbol{w}$ the solution to be found. Normally, if the two sets of centres and collocation points are identical, $\mathbf{A}$ is non-square and of dimension $N \times M$ with $M > N$. Note that in general $\mathbf{A}$ can be determined, overdetermined or underdetermined depending on the number of centres and the number of collocation points employed. The number of columns of $\mathbf{A}$, i.e. M, is decided by the number of centres m and the number of constants of integration while the number of rows N depends on the number of collocation points n.

2.2 Linear least squares problem

The goal here is to find the solution $\boldsymbol{w}$ of the Linear Least Squares (LLS) problem (9). The problem has a unique solution or infinitely many solutions depending on the characteristic of a matrix $\mathbf{A} \in \mathbf{R}^{N \times M}$. In the case of $N \geq M$ and $\mathbf{A}$ has full rank then $\mathbf{A}\boldsymbol{w} = \boldsymbol{y}$ has a unique solution. Otherwise, if $\mathbf{A}$ is rank deficient, there exist infinitely many solutions and the minimum norm L_2 solution $\min \|x\|_2$ is usually the required solution to the LLS problem. In the case of $N < M$, there exist infinitely many solutions to the underdetermined linear system $\mathbf{A}\boldsymbol{w} = \boldsymbol{y}$, but the LLS problem still has a unique minimum norm L_2 solution where the combination of "irrelevant" basis functions if existed will be driven down to a small value rather than pushed up to delicately cancelling infinities. The Singular Value Decomposition (SVD) of a matrix $\mathbf{A}$ is a matrix decomposition of great theoretical and practical importance for the treatment of least squares problem and becomes a main tool in numerous application areas [Bjorck (1996)]. SVD produces a solution that is the best approximation in the least-squares sense for an overdetermined system, or a solution whose values are smallest in the least-squares sense for an underdetermined system [Press, Flannery, Teukolsky and Vetterling (1988)] and will be employed in the present IRBFN procedure. Let p be $\min(M,N)$, the singular value decomposition of $\mathbf{A}$ can be written in the form

$$\mathbf{A} = \mathbf{U}\mathbf{\Sigma}\mathbf{V}^T = \sum_{i=1}^{p} \mathbf{u}_i \sigma_i \mathbf{v}_i^T, \quad (10)$$

where $\mathbf{U} = (\mathbf{u}_1, \ldots, \mathbf{u}_p)$ and $\mathbf{V} = (\mathbf{v}_1, \ldots, \mathbf{v}_p)$ are orthogonal matrices and $\mathbf{\Sigma} = \mathrm{diag}(\sigma_1, \ldots, \sigma_p)$ has non-negative diagonal elements appearing in non-increasing order such that

$$\sigma_1 \geq \sigma_2 \geq \ldots \geq \sigma_p. \quad (11)$$

The condition number of $\mathbf{A}$ is defined as the ratio between the largest and smallest singular values σ_1/σ_p. If this ratio is large then $\mathbf{A}$ is ill-conditioned. It is observed that the condition number of matrix $\mathbf{A}$ is larger with increasing number of centres. In all of numerical examples studied in this paper, the two sets of centres and collocation points are the same and the number of centres employed is chosen in such a manner that the matrix $\mathbf{A}$ obtained is well conditioned.

2.3 Numerical examples

A measure of the relative error of the solution or the norm of the error of the solution, N_e, is defined as

$$N_e = \sqrt{\frac{\sum_{i=1}^{n}(u_e(\boldsymbol{x}^{(i)}) - u(\boldsymbol{x}^{(i)}))^2}{\sum_{i=1}^{n} u_e(\boldsymbol{x}^{(i)})^2}}, \tag{12}$$

where $u(\boldsymbol{x}^{(i)})$ and $u_e(\boldsymbol{x}^{(i)})$ are the calculated and exact solution at the point i respectively and n is the number of collocation points.

2.3.1 Example 1 - 1D linear Poisson's equation

Consider the following 1D second order equation

$$\nabla^2 u = -16\pi^2 \sin(4\pi x) \tag{13}$$

defined on $0 \le x \le 1$ with $u = 2$ at $x = 0$ and $x = 1$. The exact solution can be verified to be

$$u_e(x) = 2 + \sin(4\pi x). \tag{14}$$

A set of 51 points distributed uniformly on the computational domain $0 \le x \le 1$ is chosen to be the set of centres and also the set of collocation points. As mentioned above, the interior collocation points are forced to satisfy the DEs while the boundary collocation points are to satisfy both the DEs and the boundary conditions. In order to assess the performance of the present TPS-IRBFN method, the Direct RBFN (DRBFN) method [Mai-Duy and Tran-Cong (2001a)], but with the TPS replacing the MQ-RBFs is also employed. Results are displayed in Figure 1 with the error norms being $4.110e0$ and $1.805e-6$ for TPS-DRBFN and TPS-IRBFN method, respectively, where the second order TPS are used in both cases. The TPS-IRBFN method yields a very high accuracy while the opposite is true for TPS-DRBFN approach. Another scheme for TPS-DRBFN is employed where the boundary collocation points are used only for the satisfaction of the boundary conditions, resulting in a determined linear system of equations. In this case, the TPS-DRBFN result is improved with the error norm being $1.245e-3$ which is still much greater than that associated with the TPS-IRBFN method ($N_e = 1.805e-6$). In the case of the first order TPS, which is C^1 continuous, only the IRBFN method can be established and the error norm achieved is $5.051e-5$. All of the error norms are presented in Table 1 showing that the TPS-IRBFN method, especially with the second order TPS, yields much better results than the TPS-DRBFN approach.

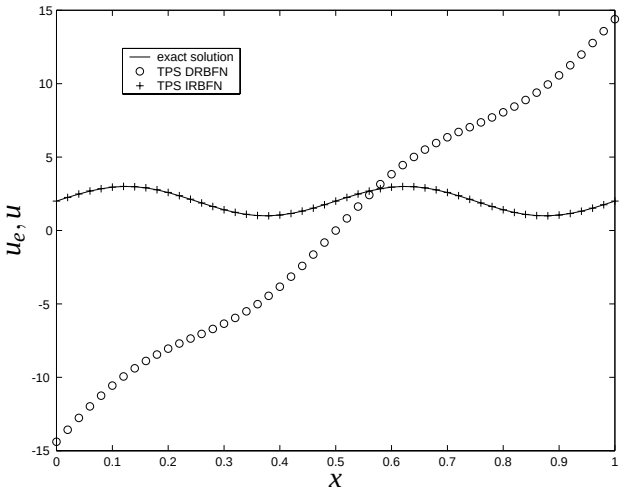

Figure 1 : Solution of $\nabla^2 u = -16\pi^2 \sin(\pi x)$: plots of the exact solution and the approximate solutions obtained from the DRBFN (non-square matrix) and IRBFN procedures with second order TPS. The centre density is 51 and uniformly distributed. The results show that the DRBFN method does not achieve an accuracy comparable with the IRBFN method.

Table 1 : 1D linear Poisson's equation: Comparison of the norm of the relative error of the solution N_e obtained by the usual TPS-DRBFN and the present TPS-IRBFN methods. Note that the DRBFN method using the first order TPS is not possible for the second order DEs because the basis function is only C^1 continuous.

N_e	$q=1$	$q=2$
DRBFN (overdetermined system)	–	4.110
DRBFN (determined system)	–	$1.245e-3$
IRBFN	$5.051e-5$	$1.805e-6$

2.3.2 Example 2 - 2D linear Poisson's equation

The problem here is to determine a function $u(x_1, x_2)$ satisfying the following PDE

$$\nabla^2 u = \sin(\pi x_1)\sin(\pi x_2) \tag{15}$$

defined on the rectangle $0 \le x_1 \le 1$, $0 \le x_2 \le 1$ subject to the Dirichlet condition $u = 0$ along the whole boundary of the domain. The exact solution is given by

$$u_e(x_1, x_2) = -\frac{1}{2\pi^2}\sin(\pi x_1)\sin(\pi x_2). \tag{16}$$

Four centre densities of 5×5, 10×10, 15×15 and 20×20 are employed to verify the present method. Results for the second order TPS-DRBFN are shown in Table 2 from which it can be seen that the results corresponding to the determined system are more accurate than those corresponding to the overdetermined system. Tables 2 and 3 show that the TPS-IRBFN method, especially with the second order TPS, yields better accuracy than the TPS-DRBFN approach. The rate of convergence of the TPS-IRBFN method can be estimated via a plot of the error norm versus the density space. A set of 41 test points are employed to compute the error norms for four different centre densities. The solution converges apparently as $h^{4.479}$ where h is the centre spacing (Figure 2).

2.3.3 Example 3 - 2D nonlinear Poisson's equation

Thermal conduction with nonlinear heat generation is considered in this example. The temperature distributing in a homogeneous solid can be described by the following PDE

$$\nabla^2 T = f(T). \tag{17}$$

In the present work, the heat generation is given by an exponential function of temperature $f(T) = -0.5\exp(T)$ which is the same as in Zheng and Phan-Thien (1992). A square domain with dimensions $[0,1] \times [0,1]$ is chosen for analysis. The boundary condition $T = 1$ is prescribed along two sides $x_1 = 0$ and $x_2 = 0$ and the adiabatical condition $\partial T/\partial n = 0$ along the other two sides $x_1 = 1$ and $x_2 = 1$ where n is the coordinate direction of the unit outward normal vector at the boundary. In order to deal with the nonlinear term $f(T)$, the iterative procedure is employed according to the following steps

1. Render the nonlinear term linear by using the temperature field obtained from the previous iteration.

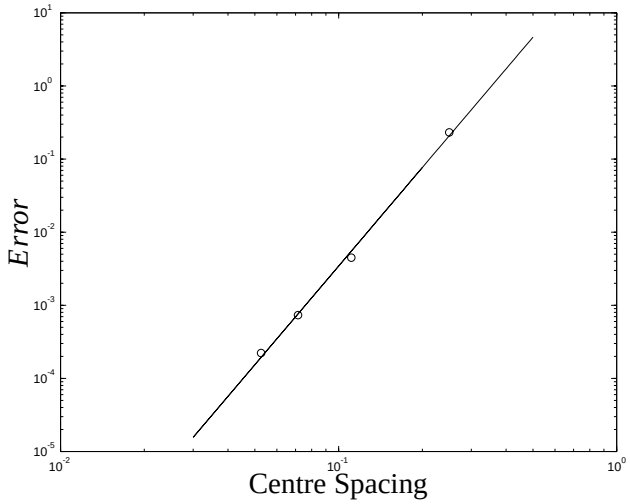

Figure 2 : Solution of $\nabla^2 u = -16\pi^2\sin(\pi x)$: the rate of convergence with centre density refinement. The errors here are defined as norms of the relative error between the exact solution and the computed solutions for the cases of density 5×5, 10×10, 15×15 and 20×20 based on the same set of 41×41 test points. The solution converges apparently as $h^{4.479}$ where h is the centre spacing.

Table 2 : 2D linear Poisson's equation: Error norms N_es of the solution obtained by the DRBFN method with second order TPS.

Density	N_e (overdetermined system)	N_e (determined system)
5×5	2.819	$3.382e-2$
10×10	2.529	$5.413e-3$
15×15	2.297	$1.787e-3$
20×20	2.062	$7.770e-4$

Table 3 : 2D linear Poisson's equation: Error norms N_es of the solution obtained by the IRBFN method with first and second order TPSs.

Density	N_e (first order)	N_e (second order)
5×5	$7.447e-3$	$1.070e-3$
10×10	$3.507e-4$	$3.726e-5$
15×15	$6.396e-5$	$4.405e-6$
20×20	$1.950e-5$	$9.853e-7$

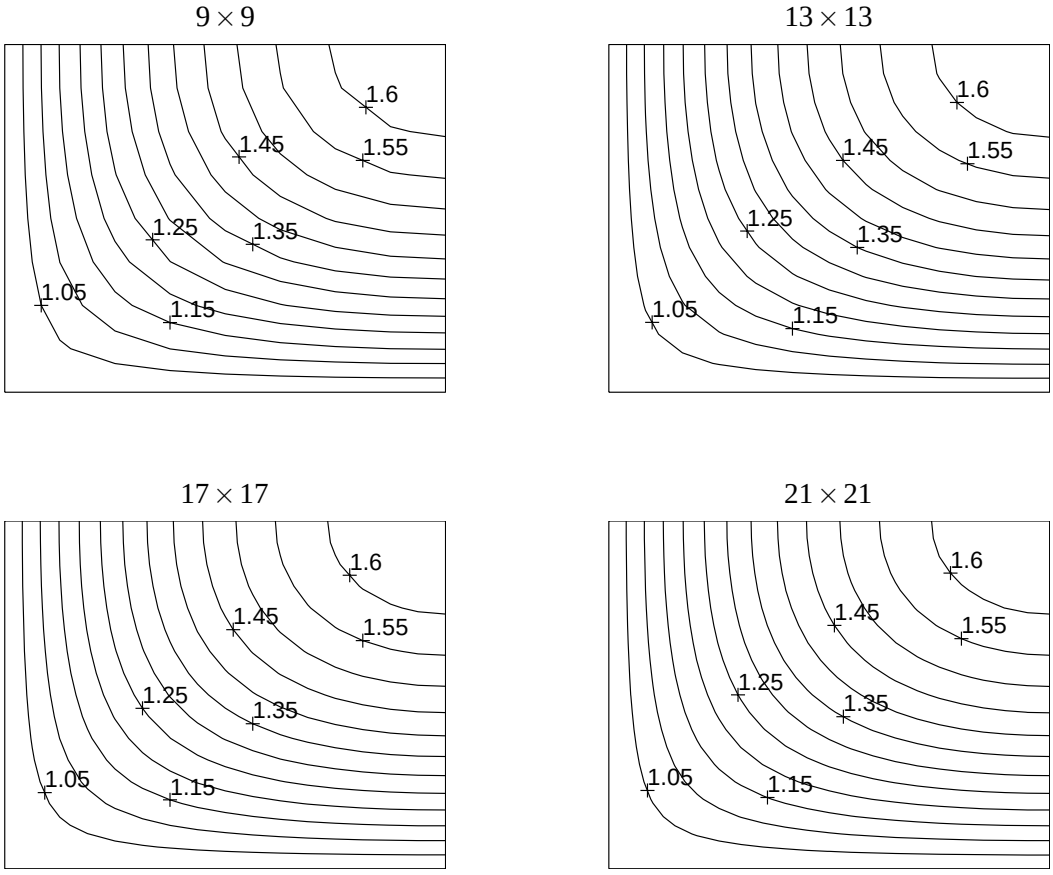

Figure 4 : Solution of $\nabla^2 T = -0.5\exp(T)$: plots of the distribution of temperature obtained by the IRBFN method with second order TPS corresponding to four different centre densities.

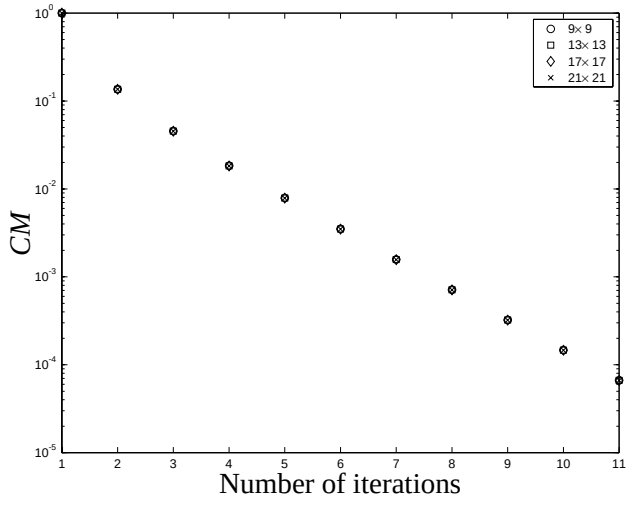

Figure 3 : Solution of $\nabla^2 T = -0.5\exp(T)$: Convergence measure based on the norm of the difference of the temperature field between two successive iterations.

Note that for the first iteration the initial temperature field needs to be guessed (in the present work it is simply initialized to zero);

2. Apply the TPS-IRBFN procedure to obtain the new estimate of the temperature field;

3. Compute the convergence measure *CM* defined as

$$CM = \sqrt{\frac{\sum_{i=1}^{n}(T^k(\boldsymbol{x}^{(i)}) - T^{k-1}(\boldsymbol{x}^{(i)}))^2}{\sum_{i=1}^{n}(T^k(\boldsymbol{x}^{(i)}))^2}},$$

where k denotes the current iteration and n is the number of collocation points;

4. Check for convergence. If $CM < tol$ where tol is a set tolerance, the solution procedure is terminated. Otherwise, repeat from the step 1.

Four centre densities, namely 9×9, 13×13, 17×17 and 21×21, are employed. With the tol set to $1.0e-4$, all

cases converge after 11 iterations (Figure 3) with the resulting temperature fields displayed in Figure 4. It can be seen that there is a good agreement between the temperature fields obtained from four centre densities employed. Another way to estimate the convergence of the iterative procedure is to use the norm of temperature [Zheng and Phan-Thien (1992)] which is defined as

$$N_T = \sqrt{\frac{\sum_{i=1}^{n} T_i^2}{n}}.$$

Figure 5 shows the norm of temperature N_T versus the number of iterations. The change of N_T is very small at the iteration number 11 where the solution can be regarded as convergent. In order to estimate the rate of convergence with mesh refinement, the solution corresponding to the finest centre density 21×21 is taken to be "exact". Results for lower centre densities are mapped onto the grid points 21×21 by IRBFN interpolation, from which the norm of the error relative to the "exact" solution is calculated. A plot of these errors is shown in Figure 6 as a function of the grid spacing h. The solution converges apparently as $h^{2.1041}$.

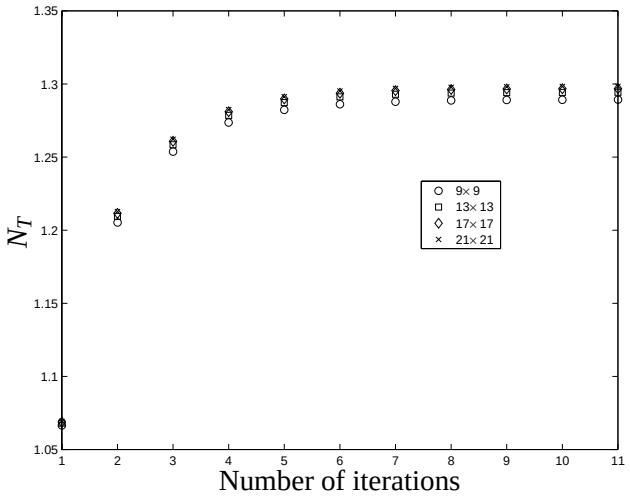

Figure 5 : Solution of $\nabla^2 T = -0.5\exp(T)$: Convergence measure based on the norm of the temperature field N_T.

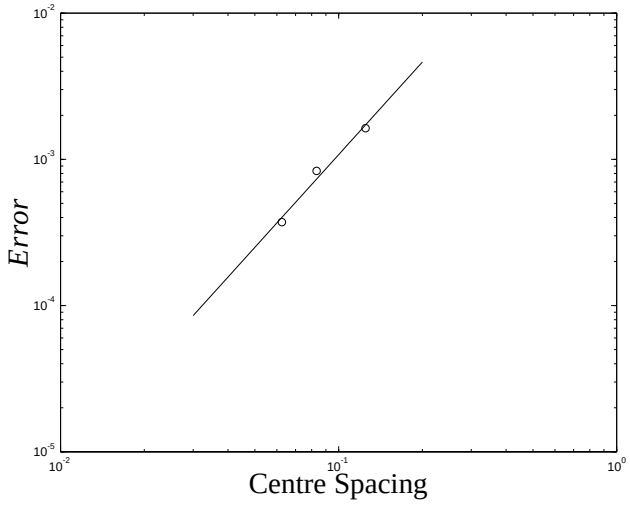

Figure 6 : Solution of $\nabla^2 T = -0.5\exp(T)$: the rate of convergence with centre density refinement. The solution corresponding to the case of 21×21 is assumed to be "exact". The errors here are defined as the norms of the error computed on the 21×21 test points between the "exact" solution and the approximate solutions from the cases of density of 9×9, 13×13 and 17×17. The solution converges apparently as $h^{2.1041}$ where h is the centre spacing.

2.3.4 Example 4 - Parabolic PDE

The problem under consideration here is governed by

$$\frac{1}{K}\frac{\partial u(\boldsymbol{x},t)}{\partial t} + g(\boldsymbol{x},t) = \nabla^2 u(\boldsymbol{x},t), \quad \boldsymbol{x} \in \Omega, \quad t > 0, \quad (18)$$

where Ω is the domain of analysis $[0,1] \times [0,1]$, K is a positive constant and g is the forcing function. In the present work, $K = 1$ and

$$g(\boldsymbol{x},t) = \sin(x_1)\sin(x_2)(2\sin(t)\cos(t))$$

as in Ingber and Phan-Thien (1992). The initial and boundary conditions yield the following solution

$$u(\boldsymbol{x},t) = \sin(x_1)\sin(x_2)\sin(t).$$

A method of discretisation in space-time is employed whereby the spatial variables are discretised using the TPS-IRBFN procedure and time is discretised using the finite difference method. Only first order finite difference approximation for the time derivative is considered in this work

$$\frac{\partial u_{(n)}}{\partial t} \approx \frac{u_{(n)} - u_{(n-1)}}{\Delta t}, \quad (19)$$

where Δt is the time step and $u_{(n)} = u(\boldsymbol{x}, t_{(n)} = n\Delta t)$. Substitution of (19) into (18) yields

$$\nabla^2 u_{(n)} - \kappa^2 u_{(n)} = g_{(n)} - \kappa^2 u_{(n-1)}, \tag{20}$$

where $\kappa^2 = 1/(K\Delta t)$. With $u_{(n-1)}$ already known from the previous step $t_{(n-1)}$, the PDE with the unknown $u_{(n)}$ can be solved by the TPS-IRBFN method. Two centre densities 6×6 and 11×11 are employed. Results at the interior point $x_1 = 0.8$ and $x_2 = 0.8$ for the coarse and fine densities using a time step of 0.25 are displayed in Table 4. The results of the two cases are close to the exact solution. The results for the fine density is slightly better than those for the coarse density as expected. Results at the interior point $x_1 = 0.3$ and $x_2 = 0.7$ generated using the fine mesh and for two different time steps are displayed in Table 5. The results using the smaller time steps are seen to be more accurate. Figure 7 shows a good agreement between the exact and approximate solutions at time $t = 8$.

Table 4 : 2D parabolic PDE: Results by the IRBFN method with second order TPS for the interior point $x_1 = 0.8$ and $x_2 = 0.8$.

Time	TPS-IRBFN, $\Delta t = 0.25$		Analytic
	6×6	11×11	
0.25	0.127073	0.127075	0.127314
0.50	0.246100	0.246103	0.246712
0.75	0.349809	0.349813	0.350771
1.00	0.431766	0.431772	0.433020
1.25	0.486877	0.486884	0.488347
1.50	0.511717	0.511725	0.513310
1.75	0.504741	0.504748	0.506358
2.00	0.466382	0.466389	0.467924
2.25	0.399026	0.399032	0.400396
2.50	0.306861	0.306865	0.307973
2.75	0.195616	0.195619	0.196402
3.00	0.072209	0.072210	0.072620
3.25	-0.055687	-0.055688	-0.055677
3.50	-0.180122	-0.180124	-0.180512
3.75	-0.293357	-0.293361	-0.294125
4.00	-0.388353	-0.388358	-0.389450

Table 5 : 2D parabolic PDE: Results by the IRBFN method with second order TPS for the interior point $x_1 = 0.3$ and $x_2 = 0.7$.

Time	TPS-IRBFN, 11×11		Analytic
	$\Delta t = 0.5$	$\Delta t = 0.25$	
0.50	0.0904	0.0907	0.0912
1.00	0.1582	0.1591	0.1601
1.50	0.1872	0.1885	0.1899
2.00	0.1703	0.1717	0.1731
2.50	0.1118	0.1129	0.1139
3.00	0.0258	0.0264	0.0268
3.50	-0.0663	-0.0664	-0.0667
4.00	-0.1424	-0.1431	-0.1440
4.50	-0.1835	-0.1847	-0.1861
5.00	-0.1797	-0.1811	-0.1825
5.50	-0.1319	-0.1332	-0.1343
6.00	-0.0518	-0.0526	-0.0531
6.50	0.0409	0.0408	0.0409
7.00	0.1237	0.1243	0.1250
7.50	0.1762	0.1773	0.1785
8.00	0.1855	0.1869	0.1883

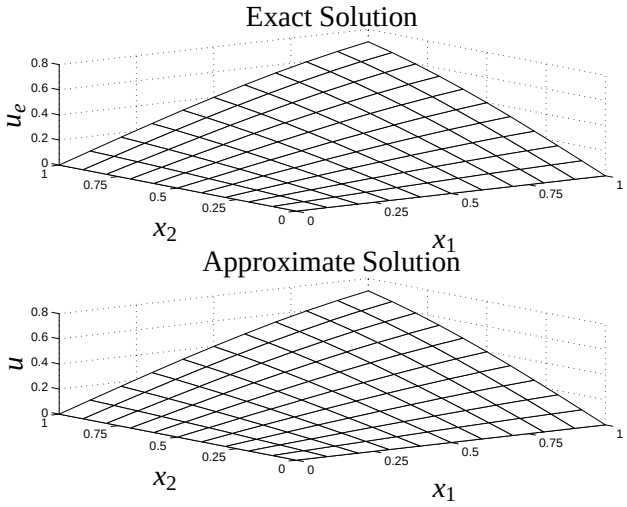

Figure 7 : Solution of Parabolic PDE by the IRBFN with second order TPS using a centre density of 11×11: plots of exact solution and approximate solution at the time $t = 8$.

2.3.5 Example 5 - 3D linear Poisson's equation

The problem here is to determine a function $u(x_1,x_2,x_3)$ satisfying the following PDE

$$\nabla^2 u = -\left(\frac{\partial u}{\partial x_1}+\frac{\partial u}{\partial x_2}+\frac{\partial u}{\partial x_3}\right) \tag{21}$$

defined on the cube $0 \le x_1 \le 1$, $0 \le x_2 \le 1$, $0 \le x_3 \le 1$ subject to the Dirichlet condition $u = \exp(-x_1)+\exp(-x_2)+\exp(-x_3)$ on the whole boundary of the domain. The exact solution is given by

$$u_e(x_1,x_2,x_3) = \exp(-x_1)+\exp(-x_2)+\exp(-x_3). \tag{22}$$

Three centre densities of $3\times3\times3$, $5\times5\times5$ and $7\times7\times7$ are employed to verify the present method. Results for the first order TPS-DRBFN are shown in Table 6 from which it can be seen that the applicability of the TPS $R^{2q}\log(R)$ in 3D is also verified and the method exhibits excellent mesh-convergence.

Table 6 : 3D linear Poisson's equation: Error norms N_es of the solution obtained by the IRBFN method with first order TPS.

Density	N_e
$3\times3\times3$	$1.301e-4$
$5\times5\times5$	$5.525e-6$
$7\times7\times7$	$9.405e-7$

3 TPS-IRBFN method in curvilinear coordinates

3.1 Numerical formulation

For problems on polar or cylindrical domains, it may be more efficient to use curvilinear coordinates and the aim here is to demonstrate the working of the present method in such situations. For 2D problems, the first step is to transform the rectangular coordinates into the convenient polar or cylindrical coordinates. Consider the thin plate splines

$$g^{(i)}(x_1,x_2) = R^{2q}\log(R),$$

where q is the order of the TPS and R is the Euclidean distance between the ith centre $\boldsymbol{c}^{(i)}$ and the collocation point $\boldsymbol{x}$, i.e. $R = \|\boldsymbol{c}^{(i)}-\boldsymbol{x}\|_2$. Applying the polar coordinate transformation, $x_1 = r\cos(\theta)$, $x_2 = r\sin(\theta)$, where $r = \sqrt{x_1^2+x_2^2}$ and $\theta = \arctan(x_2/x_1)$, then TPS becomes

$$\begin{aligned} g^{(i)}(r,\theta) = &\left\{\left[(r\cos(\theta)-r^{(i)}\cos(\theta^{(i)})\right]^2+\right.\\ &\left.\left[r\sin(\theta)-r^{(i)}\sin(\theta^{(i)})\right]^2\right\}^q\\ &\log\left(\left\{\left[(r\cos(\theta)-r^{(i)}\cos(\theta^{(i)})\right]^2+\right.\right.\\ &\left.\left.\left[r\sin(\theta)-r^{(i)}\sin(\theta^{(i)})\right]^2\right\}^{1/2}\right) \end{aligned} \tag{23}$$

Similarly, this transformation can also be used to obtain the new forms of the governing equations and the associated boundary conditions in polar coordinates. For example, in polar coordinates, the Poisson's equation (5) now takes the form

$$\frac{\partial^2 u}{\partial r^2}+\frac{1}{r}\frac{\partial u}{\partial r}+\frac{1}{r^2}\frac{\partial^2 u}{\partial\theta^2} = p(r,\theta). \tag{24}$$

The corresponding *SSE* which is employed in designing the networks for obtaining numerical solution of (5), (6) and (7) can be written in polar coordinates as follows

$$\begin{aligned} SSE \;=\; &\sum_{(i)\in\Omega}\left[\left(u^{(i)}_{,rr}+\frac{u^{(i)}_{,r}}{r^{(i)}}+\frac{u^{(i)}_{,\theta\theta}}{r^{(i)2}}\right)-p^{(i)}\right]^2+\\ &\sum_{(i)\in\Omega}\left[u^{(i)}_r-u^{(i)}_\theta\right]^2+\sum_{(i)\in\Gamma_1}\left[u^{(i)}_r-p^{(i)}_1\right]^2+\\ &\sum_{(i)\in\Gamma_2}\left[\left(n^{(i)}_r u^{(i)}_{,r}+n^{(i)}_\theta\frac{u^{(i)}_{,\theta}}{r^{(i)}}\right)-p^{(i)}_2\right]^2, \end{aligned} \tag{25}$$

where the term u_r is obtained via $u_{,rr}$ and u_θ via $u_{,\theta\theta}$.

The second step, for the indirect RBFN methodology, is to integrate the TPS in (23) with respect to r and θ to obtain new basis functions for lower order derivatives and the function itself. Unfortunately, only the integrations of the TPS in (23) with respect to r can be found explicitly. On the other hand, the integrations of the TPS with respect to θ need to be performed numerically. The following is the general scheme to compute new basis functions for lower derivatives and function using numerical integrations. Let k be the highest order of the derivative of the function u in the DEs and t be the variable under

consideration, then the function u and its derivatives are expressed in terms of basis functions as

$$\frac{\partial^k u}{\partial t^k}(t) = \sum_{i=1}^{m} w^{(i)} g^{(i)}(t), \tag{26}$$

$$\frac{\partial^{k-1} u}{\partial t^{k-1}}(x) - \frac{\partial^{k-1} u}{\partial t^{k-1}}(a) = \sum_{i=1}^{m} w^{(i)} \int_a^x g^{(i)}(t)dt, \tag{27}$$

$$\frac{\partial^{k-2} u}{\partial t^{k-2}}(x) - \frac{\partial^{k-2} u}{\partial t^{k-2}}(a) = \sum_{i=1}^{m} w^{(i)} \int_a^x dt_2 \int_a^{t_2} g^{(i)}(t)dt, \tag{28}$$

.....

$$\frac{\partial u}{\partial t}(x) - \frac{\partial u}{\partial t}(a) = \sum_{i=1}^{m} w^{(i)} \int_a^x dt_{k-1} \ldots \int_a^{t_3} dt_2 \int_a^{t_2} g(t)dt, \tag{29}$$

$$u(x) - u(a) = \sum_{i=1}^{m} w^{(i)} \int_a^x dt_k \int_a^{t_k} dt_{k-1} \ldots \int_a^{t_3} dt_2 \int_a^{t_2} g(t)dt, \tag{30}$$

where a and x are two reference collocation points, g is the TPS basis function. The iterated integrals of function g over the finite interval between two collocation points a and x can be simplified to [Abramowitz and Stegun (1972)]

$$\int_a^x dt_k \int_a^{t_k} dt_{k-1} \ldots \int_a^{t_3} dt_2 \int_a^{t_2} g(t)dt = \frac{(x-a)^k}{(k-1)!} \int_0^1 t^{k-1} g(x-(x-a)t)dt. \tag{31}$$

Clearly, the integral on the RHS of (31) can be handled easily by using numerical integration schemes. One of the most popular numerical integration schemes is the Gaussian quadrature one, whereby the integrand is simply evaluated at some discrete points. In the present investigation, a Gaussian quadrature of 5 points is employed.

3.2 Numerical examples

3.2.1 Example 1 - Poisson's equation on unit disk

The problem formulation is given by

$$\nabla^2 u = -1, \qquad \mathbf{x} \in \Omega, \tag{32}$$

where Ω is the unit disk, subject to the boundary condition $u = 0$ on the boundary $\partial\Omega$. The exact solution is given by

$$u = \frac{1 - x_1^2 - x_2^2}{4}.$$

It is convenient to solve this problem in polar coordinates. Three discretisation schemes for both the FEM and IRBFN method are shown in Figure 8 where the RBF centres are distributed uniformly in radial and tangential directions. The representations for u and its derivatives using the second order TPS in polar coordinates are substituted into (25) which is then collocated according to the set of data points chosen resulting in a linear system of equations. In order to evaluate the performance of the present IRBFN method, FEM is also employed to solve the same problem using nearly equal numbers of DOF (Figure 8 and Table 7). Note that the FEM results here are obtained using the PDE tool in MATLAB. The IRBFN method achieves a higher accuracy than the FEM (Table 7) and its convergence rate is also faster as shown in Figure 9 where the IRBFN method converges as $d^{3.05}$ while the FEM only as $d^{1.11}$ where d is the number of DOF.

Table 7 : Poisson's equation on unit disk: Meshes and results by FEM and the IRBFN method.

FEM			IRBFN	
Nodes	Triangles	N_e	Centres	N_e
103	172	5.6653e-3	100	$4.8712e-3$
200	358	2.7711e-3	196	$5.0875e-4$
363	668	1.3985e-3	361	$9.7398e-5$

3.2.2 Example 2 - Jeffery-Hamel flow

The IRBFN method in polar coordinates is verified further with the simulation of the Jeffery-Hamel problem. This problem, which has a wide range of engineering and environmental applications, poses a classical problem

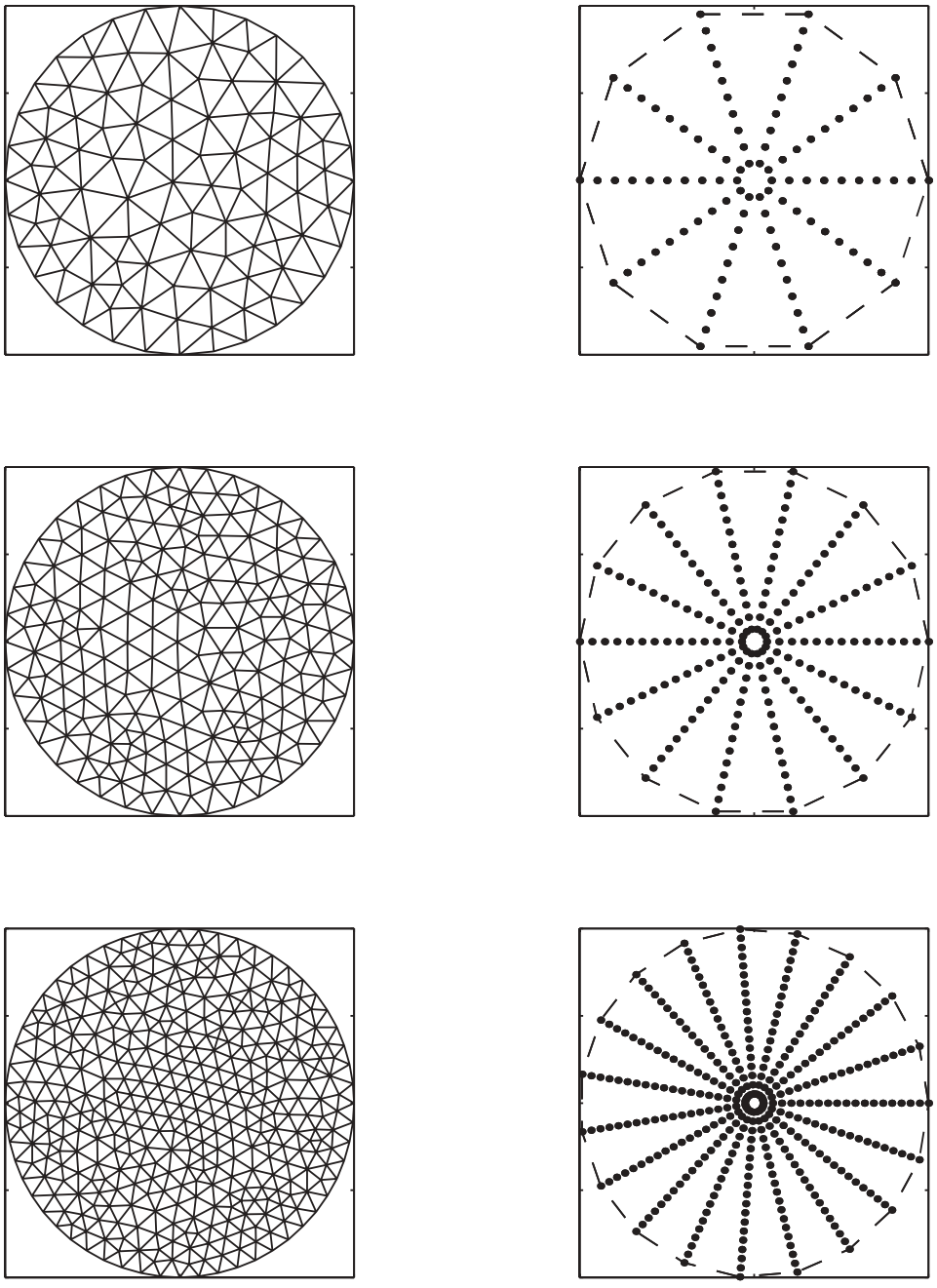

Figure 8 : Poisson's equation on unit disk: Meshes and data densities used in the FEM (left) and IRBFN method (right) respectively with nearly equal number of DOF between the two methods.

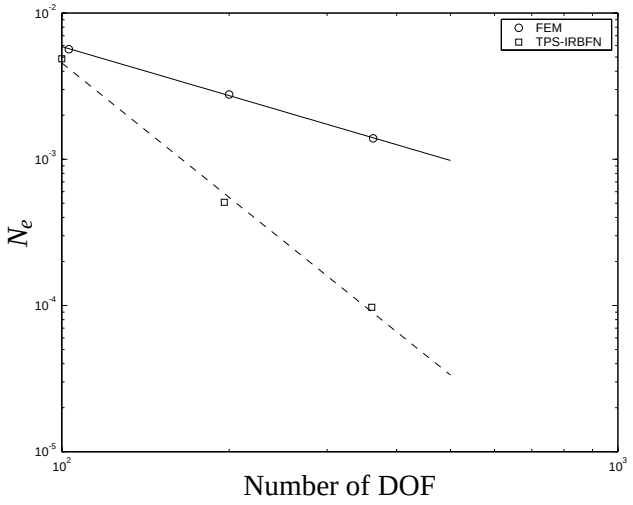

Figure 9 : Poisson's equation on unit disk: Convergence rates by the FEM and IRBFN methods. Legends ○: FEM and □: IRBFN. The convergence rates are as $d^{1.11}$ and $d^{3.05}$ for FEM and IRBFN respectively where d is the number of DOF.

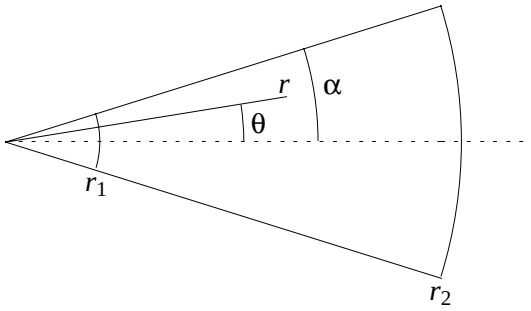

Figure 10 : Jeffery-Hamel problem: geometry.

discussed in many textbooks [Batchelor (1967)]. The two-dimensional steady convergent flow of a viscous, incompressible fluid between two semi-infinite plane walls set at an angle 2α is considered here. The inward flow is driven by a steady line sink of strength Q at the apex. As pointed out by Bush and Tanner (1983), the Jeffery-Hamel flow problem provides a means of testing numerical solution schemes since it is a steady state flow in which the inertia terms do not vanish identically (as they do in flow between infinite parallel plates or Poiseuille flow) and an exact solution can be obtained for comparison with numerical results. For these reasons the Jeffery-Hamel problem was used as a test example by Gartling, Nickell and Tanner (1977) in finite element convergence study, Bush and Tanner (1983) and Zheng, Phan-Thien and Coleman (1991) in boundary element convergence study. Here, this problem is also selected as a representative case to assess the performance of the IRBFN method. Consider a system of polar coordinates (r,θ) centred at the point of intersection of the walls. In this coordinates system, the velocity components of the fluid are denoted as u_r and u_θ respectively. The 2D domain of analysis is shown in Figure 10 as a sector set at $\theta = \pm\alpha = \pm\pi/6$ with the inlet as an arc at r_1 and the outlet as an arc at r_2. The velocity distribution is symmetrical about the centreline $\theta = 0$. Owing to symmetry, only one half domain is considered. It is convenient to use the streamfunction ψ defined by

$$u_r = -\frac{1}{r}\frac{\partial\psi}{\partial\theta}, \quad u_\theta = \frac{\partial\psi}{\partial r}.$$

Then the vorticity can be written as

$$\xi = \nabla^2\psi \tag{33}$$

and for a steady, laminar and isothermal flow, the Navier-Stokes equations reduce to the vorticity equation

$$\rho\left(-\frac{1}{r}\frac{\partial\psi}{\partial\theta}\frac{\partial\xi}{\partial r} + \frac{1}{r}\frac{\partial\psi}{\partial r}\frac{\partial\xi}{\partial\theta}\right) = \mu\nabla^2\xi, \tag{34}$$

where μ is the viscosity, ρ is the density and the Laplacian in cylindrical polar coordinates is $\nabla^2 = \partial^2/\partial r^2 + (1/r)\partial/\partial r + (1/r^2)\partial^2/\partial\theta^2$. The no-slip condition is imposed at the wall as

$$\frac{\partial\psi}{\partial r} = 0, \quad \frac{\partial\psi}{\partial\theta} = 0 \quad \text{at} \quad \theta = \alpha,$$

while the symmetry condition is enforced on the centreline, which yields

$$\psi = 0, \quad \xi = 0 \quad \text{at} \quad \theta = 0.$$

At the inlet $r = r_1$ and the outlet $r = r_2$, the boundary conditions $\partial\psi/\partial r$ and $\partial\psi/\partial\theta$ can be chosen as functions of θ

in a manner consistent with the given flux Q. For convenience, the variables are non-dimensionlised as follows

$$r' = \frac{r}{r_1}, \quad \psi' = \frac{\psi}{(1/2)Q},$$
$$u_i' = \frac{(1/2)Q}{r_1} u_i \quad \text{and} \quad \xi' = \frac{r_1^2}{(1/2)Q}\xi. \tag{35}$$

From here on, the primes are dropped for brevity. The governing equations can be written as

$$\xi = \nabla^2 \psi, \tag{36}$$
$$Re\left(-\frac{1}{r}\frac{\partial\psi}{\partial\theta}\frac{\partial\xi}{\partial r} + \frac{1}{r}\frac{\partial\psi}{\partial r}\frac{\partial\xi}{\partial\theta}\right) = \nabla^2\xi, \tag{37}$$

where $Re = Q/(2\nu)$ is the Reynolds number and $\nu = \mu/\rho$ is the kinematic viscosity.

Closed form solution

In this case the domain is semi-infinite and it is not necessary to use the boundary conditions at the inlet and the outlet as defined by the finite size domain. Following Jeffery and Hamel [Batchelor (1967)], the flow is assumed to be purely radial which yields self-similar velocity profiles at all radii and, as a consequence, the streamfunction ψ depends only on θ. Then, equation (37) gives

$$\frac{d^4\psi}{d\theta^4} + 4\frac{d^2\psi}{d\theta^2} - 2Re\frac{d\psi}{d\theta}\frac{d^2\psi}{d\theta^2} = 0 \tag{38}$$

subject to boundary conditions

$$\psi(\pm\alpha) = \pm 1 \quad \text{and} \quad \frac{d\psi}{d\theta}(\pm\alpha) = 0 \tag{39}$$

for the case of full domain or,

$$\psi(\alpha) = 1,\ \frac{d\psi}{d\theta}(\alpha) = 0,\ \psi(0) = 0,\ \text{and}\ \frac{d^2\psi}{d\theta^2}(0) = 0 \tag{40}$$

for the case of one half domain. For this nonlinear fourth order ODE, only the closed form solution corresponding to zero or very large Reynolds numbers can be found analytically and hence the solution corresponding to low and medium Reynolds numbers must be solved numerically. Gartling, Nickell and Tanner (1977) used an iterative numerical quadrature process to estimate the "exact" solution of Jeffery-Hamel flow. The procedure provides updated approximations of the Reynolds number until the computed flux matches the prescribed flux with given values of α, ρ, μ and the flow rate per unit length Q. Here, the IRBFN method using second order TPS will be employed for the numerical solution of (38) and (39) and the results obtained will be compared with the exact solution for two extreme cases of Reynolds number. Note that this computed IRBFN solution will be regarded as the closed form solution of the Jeffery-Hamel flow in the next section. Following are the two closed form solutions corresponding to $Re = 0$ and $Re \to \infty$ respectively. In the case of creeping flow (zero Reynolds number), equation (38) reduces to

$$\frac{d^4\psi}{d\theta^4} + 4\frac{d^2\psi}{d\theta^2} = 0 \tag{41}$$

and the corresponding exact solution is

$$\psi = \frac{2\cos(2\alpha)\theta - \sin(2\theta)}{2\alpha\cos(2\alpha) - \sin(2\alpha)}. \tag{42}$$

From (42), the ratio between the radial velocity u_r and the centreline radial velocity u_0, which is independent of radius r and the flow rate Q, can be obtained as

$$\frac{u_r}{u_0} = \frac{\cos(2\theta) - \cos(2\alpha)}{1 - \cos(2\alpha)}. \tag{43}$$

In the case of large Reynolds number, the closed form solution was derived by Batchelor (1967)

$$\frac{u_r}{u_0} = 3\tanh^2\left\{\left(-\frac{1}{2}\alpha Re\right)^{\frac{1}{2}}\left(1 - \frac{\theta}{\alpha}\right) - \tanh^{-1}\left(\frac{2}{3}\right)^{\frac{1}{2}}\right\} - 2. \tag{44}$$

where Re is the Reynolds number defined as $Re = \frac{\alpha u_0 r\rho}{\mu}$ whose value is only slightly different from the Reynolds number defined in this work. Numerical solution of the second order ODE was obtained using the MQ-IRBFN method [Mai-Duy and Tran-Cong (2001a)] where basis functions for the first derivative and the function were obtained by analytical integrations. Here, to solve higher order ODE, numerical integrations are employed to construct the design matrix $\mathbf{A}$. In solving (38) and (39) with the presence of fourth order derivative, $k = \{1,2,3,4\}$ in (31) are used here to obtain basis functions for the third, second, first derivatives and the function respectively. Figure 11 displays the result for u_r/u_0 obtained by the present IRBFN method for the case of creeping flow, which is in satisfactory agreement with the exact solution. The achieved norm of the relative error of the solution is $7.48e-8$. Results obtained for $Re = 10, 50, 100, 1000, 5000$ are plotted in Figure 12 together with that by Batchelor (1967). Note that the latter which is only available for large Re is calculated at

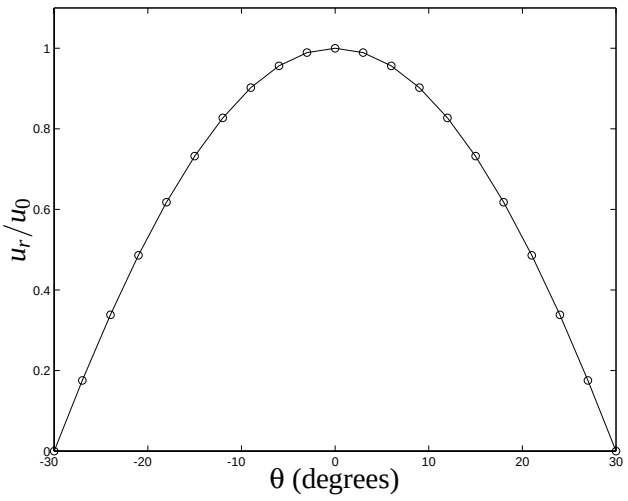

Figure 11 : Jeffery-Hamel problem: closed form solution for the case of creeping flow. Legends solid line: analytical solution and ○: IRBFN solution. There is a good agreement between the two solutions.

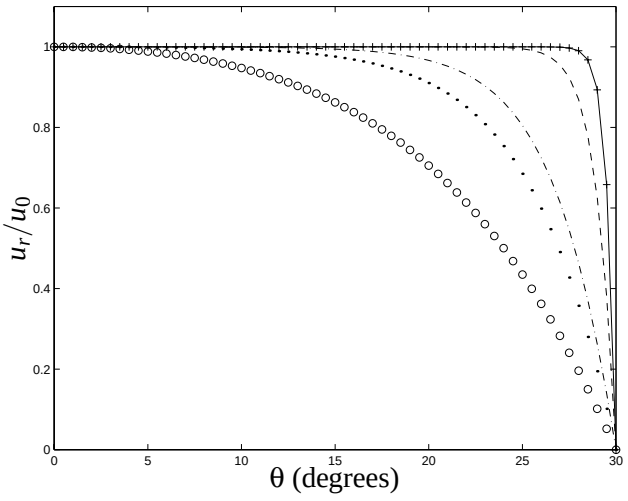

Figure 12 : Jeffery-Hamel problem: closed form solution by the present IRBFN method. Legends solid line: $Re = 5000$; dashed line: $Re = 1000$, dashdot line: $Re = 100$, ·: $Re = 50$ and ○: $Re = 10$. Result by Batchelor (1967) at $Re = 5000$ is also plotted with the legend + showing a good agreement with IRBFN result at large Reynolds number.

$Re = 5000$ here. The IRBFN closed form result is in good agreement with Batchelor's result (1967) at large Reynolds number. It can be seen that the velocity magnitude becomes nearly constant except near the plate walls when the Reynolds number increases. On the other hand, boundary layers appear at large Reynolds number.

Computed solution

Only a finite length of the wedge geometry can be modelled with the IRBFN method and the boundary conditions at the inlet and the outlet now have to be specified for the problem. To provide a strong test for the method, the velocity vector taken from the IRBFN closed form solution is applied at the inlet while the exit condition is enforced at the outlet, i.e. $\frac{\partial \psi}{\partial r}$ and $\frac{\partial \psi}{\partial \theta}$ at the inlet; $\frac{\partial \psi}{\partial n} = \frac{\partial \psi}{\partial r} = 0$ and $\frac{\partial \xi}{\partial n} = \frac{\partial \xi}{\partial r} = 0$ at the outlet where n is the coordinate direction of the unit outward normal vector at the boundary. The flow is symmetric about the centreline ($\psi = 0$ and $\xi = 0$) and no-slip conditions are prescribed at the plate wall ($\frac{\partial \psi}{\partial r} = 0$ and $\frac{\partial \psi}{\partial \theta} = 0$). Although the outlet boundary condition $\frac{\partial \xi}{\partial r} = 0$ is incorrect, it can be expected that if the domain of analysis is large enough, the disturbance introduced at the outlet is small and the Jeffery-Hamel flow can be produced in the domain except for a small region at the outlet. For this reason, r_1 and r_2 are chosen to be 1 and 7 respectively (they were chosen somewhat arbitrarily, but to give an aspect ratio

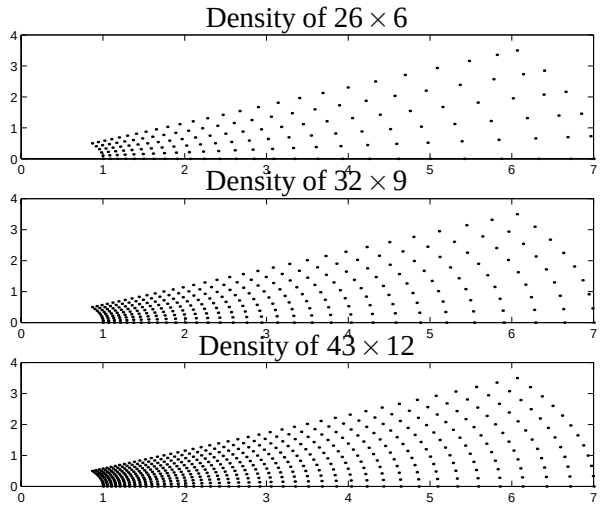

Figure 13 : Jeffery-Hamel problem: Three centre densities for each of which the distances between each centre and its neighbouring centres are nearly equal.

r_2/r_1 which is large enough for Jeffery-Hamel flow to be observed and small enough to prevent the need for expensive calculations). Three sets of centres are displayed in Figure 13 where the discretisation is uniform in the circumferential direction and non-uniform in the radial direction. The latter is characterised by the fact that the distances between each centre and its neighbouring centres are nearly equal. Iterative procedure is employed to cope with the nonlinear convective term which is similar to the iterative procedure described in section 2.3.3. The convective term is estimated using the result at the previous iteration and hence this term becomes known at the current iteration resulting in a linear least-squares problem. Note that by using this approach the design matrix **A** does not change during iteration and hence the SVD algorithm for **A** needs to be done only once. Furthermore, this decomposition can be used for any Reynolds number due to the fact that **A** does not depend on the material properties. For this problem, numerical experience shows that the first order TPS achieves a better results than the second order TPS and the results corresponding to the former are presented. With three relatively coarse centre densities employed, the IRBFN method can achieve moderate Reynolds numbers. The solution is convergent up to Reynolds numbers of 100, 150 and 200 with discretisations in tangential direction only being 6, 9 and 12 points (6, 3.75 and 2.5 degrees) respectively. It can be seen that at the Reynolds number of 200 the profile of the radial velocity is very steep near the wall. Higher Reynolds number will produce the boundary layer and a number of discretisation points in the tangential direction needs to be increased resulting in relatively large matrices. In this case it is better to use the domain decomposition technique rather than the single domain, which is to be reported in future work. The results including the variation of the radial velocity along the centreline and the profile of the radial velocity at $r \approx 3.5$ (roughly half way between the inlet and the outlet) are displayed in Figures 14-19 from which it can be seen that the agreement with the closed form solution is satisfactory. The IRBFN method can achieve Reynolds number up to $R_e = 200$ using 12 points distributed uniformly in tangential direction in comparison with *Re* up to 40 using 11 points achieved by BEM [Zheng, Phan-Thien and Coleman (1991)] and *Re* up to 1000 using 21 points by FEM [Gartling, Nickell and Tanner (1977)].

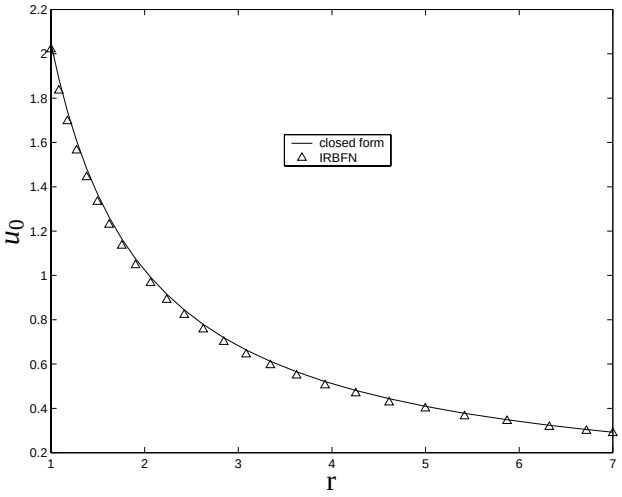

Figure 14 : Jeffery-Hamel problem, centre density of 26×6: the radial velocity obtained along the centreline at $Re = 100$

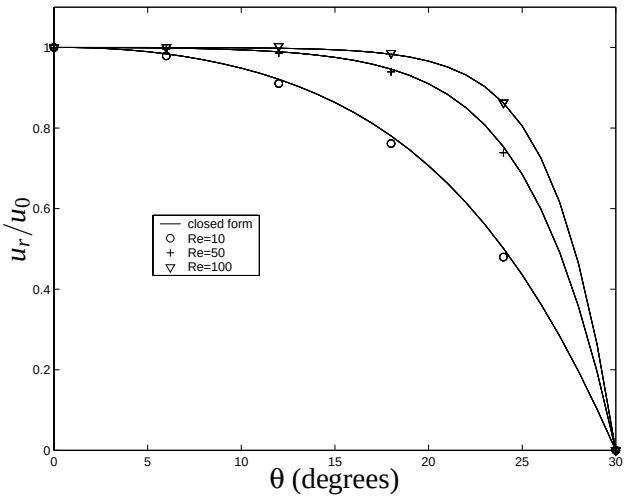

Figure 15 : Jeffery-Hamel problem, centre density of 26×6: the profile of radial velocity at $r \approx 3.5$ for Reynolds numbers of 10, 50 and 100.

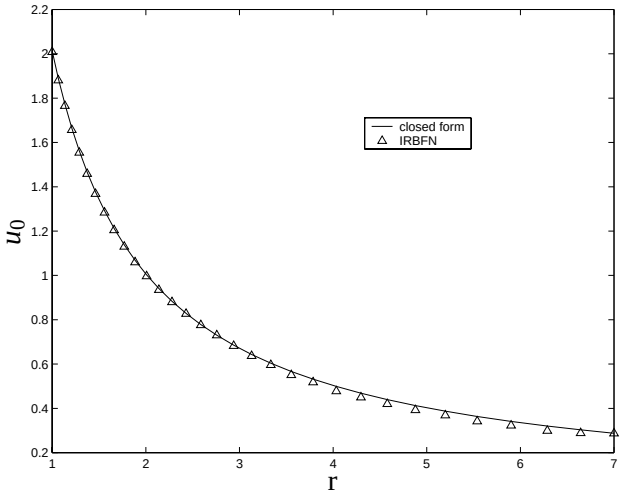

Figure 16 : Jeffery-Hamel problem, centre density of 32×9: the radial velocity obtained along the centreline at $Re = 150$

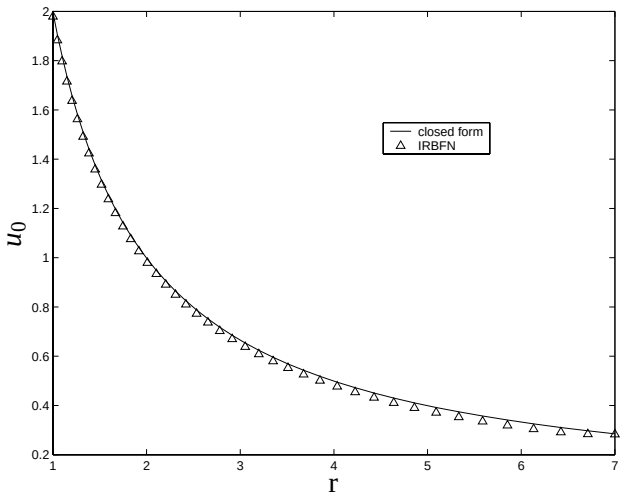

Figure 18 : Jeffery-Hamel problem, centre density of 43×12: the radial velocity obtained along the centreline at $Re = 200$

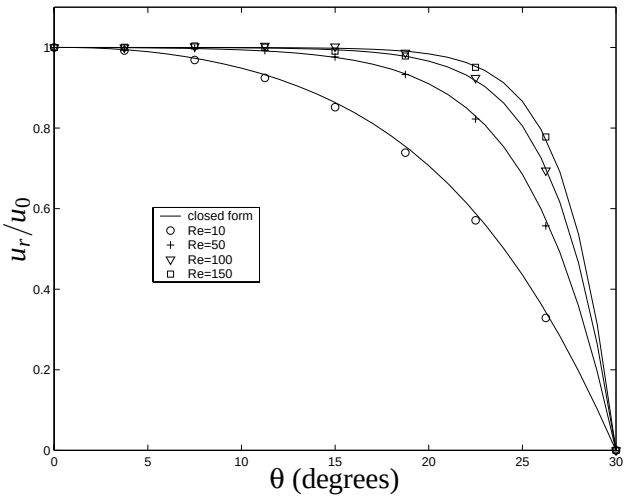

Figure 17 : Jeffery-Hamel problem, centre density of 32×9: the profile of radial velocity at $r \approx 3.5$ for Reynolds numbers of 10, 50, 100 and 150.

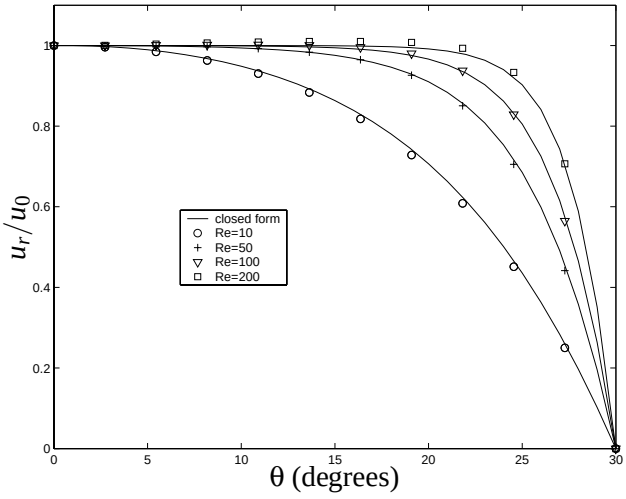

Figure 19 : Jeffery-Hamel problem, centre density of 43×12: the profile of radial velocity at $r \approx 3.5$ for Reynolds numbers of 10, 50, 100 and 200.

4 Concluding remarks

In this paper, the Indirect RBFN method using first and second order thin plate splines for numerical solution of DEs in rectangular and curvilinear coordinates is developed and verified successfully. Special attention here is given to the employment of numerical integration schemes in the IRBFN procedure where new basis functions for lower derivatives and function could not be found explicitly by analytical integrations. This scheme allows the indirect RBFN method to be general in the sense that the method can be employed with any kind of radial basis function and also in any kind of coordinates system. Furthermore, the scheme is also effective in solving higher DEs, i.e. there are no added computational difficulties relative to the case of second order DEs. Gaussian quadrature is employed throughout the study and the results obtained are accurate. The TPS-IRBFN is easy to implement and more automatic than the MQ-IRBFN method and numerical examples show that the TPS-IRBFN method achieves a high accuracy.

Acknowledgement: This work is supported by a Special USQ Research Grant (Grant No 179-310) to Thanh Tran-Cong. Nam Mai-Duy is supported by a USQ scholarship. This support is gratefully acknowledged. The authors would like to thank the referees for their helpful comments.

References

Abramowitz, M.; Stegun, I. A. (1972): *Handbook of Mathematical functions*. Dover Publications, New York.

Atluri, S. N.; Shen, S. (2002a): The meshless local Petrov-Galerkin (MLPG) method: A simple & less-costly alternative to the finite element and boundary element methods. *CMES: Computer Modeling in Engineering & Sciences*, vol. 3, pp. 11-52.

Atluri, S. N.; Shen, S. (2002b): *The Meshless Local Petrov-Galerkin Method*. Tech Science Press, Encino.

Batchelor, G. K. (1967): *An Introduction to Fluid Dynamics*. Cambridge University Press, Cambridge.

Bjorck, A. (1996): *Numerical Methods for Least Squares Prolems*. SIAM, Philadelphia.

Bush, M. B.; Tanner, R. I. (1983): Numerical solution of viscous flows using integral equation methods. *International Journal for Numerical Methods in Fluids*, vol. 3, pp. 71-92.

Dissanayake, M. W. M. G.; Phan-Thien, N. (1994): Neural-Network-Based approximations for solving partial differential equations. *Communications in Numerical Methods in Engineering*, vol. 10, pp. 195-201.

Dubal, M. R. (1994): Domain decomposition and local refinement for multiquadric approximations. I: Second-order equations in one-dimension. *Journal of Applied Science and Computation*, vol. 1(1), pp. 146-171.

Duchon, J. (1977): Splines minimizing rotation-invariant semi-norms in Sobolev spaces. In: W. Schempp and K. Zeller (eds) *Constructive Theory of Functions of Several Variables, Lecture Notes in Mathematic*, Springer-Verlag, Berlin, vol. 571, pp. 85-100.

Fornberg, B.; Driscoll, T. A.; Wright, G.; Charles, R. (2002): Observations on the behavior of radial basis function approximations near boundaries. *Computers and Mathematics with Applications*, vol. 43, pp. 473-490.

Gartling, D. K.; Nickell, R. E.; Tanner, R. I. (1977): A finite element convergence study for accelerating flow problems. *International Journal for Numerical Methods in Engineering*, vol. 11, pp. 1155-1174.

Gutmann, H. M. (2001): On the semi-norm of radial basis function interpolants. *Journal of Approximation Theory*, vol. 111, pp. 315-328.

Haykin, S. (1999): *Neural Networks: A Comprehensive Foundation*. Prentice-Hall, New Jersey.

Ingber, M. S.; Phan-Thien, N. (1992): A boundary element approach for parabolic differential equations using a class of particular solutions. *Applied Mathematical Modelling*, vol. 16, pp. 124-132.

Kansa, E. J. (1990): Multiquadrics- A scattered data approximation scheme with applications to computational fluid-dynamics-II. Solutions to parabolic, hyperbolic and elliptic partial differential equations. *Computers and Mathematics with Applications*, vol. 19(8/9), pp. 147-161.

Mai-Duy, N.; Tran-Cong, T. (2001a): Numerical solution of differential equations using multiquadric radial basis function networks. *Neural Networks*, vol. 14, pp. 185-199.

Mai-Duy, N.; Tran-Cong, T. (2001b): Numerical solution of Navier-Stokes equations using multiquadric radial basis function networks. *International Journal for*

Numerical Methods in Fluids, vol. 37, pp. 65-86.

Mai-Duy, N.; Tran-Cong, T. (2002): Mesh-free radial basis function network methods with domain decomposition for approximation of functions and numerical solution of Poisson's equations. *Engineering Analysis with Boundary Element*, vol. 26, pp. 133-156.

Press, W. H.; Flannery, B. P.; Teukolsky, S. A.; Vetterling, W. T. (1988): *Numerical Recipes in C: The Art of Scientific Computing*. Cambridge University Press, Cambridge.

Schaback, R. (1995): In: M. Daehlen; T. Lyche and L. L. Schumaker (eds) *Mathematical Methods for Curves and Surfaces*, Vanderbilt University Press, Nashville, pp. 477-496.

Sharan, M.; Kansa, E. J.; Gupta, S. (1997): Application of the multiquadric method for numerical solution of elliptic partial differential equations. *Journal of Applied Science and Computation*, vol. 84, pp. 275-302.

Takeuchi, J.; Kosugi, Y. (1994): Neural network representation of finite element method. *Neural Networks*, vol. 7(2), pp. 389-395.

Zerroukat, M.; Power, H.; Chen, C. S. (1998): A numerical method for heat transfer problems using collocation and radial basis functions. *International Journal for Numerical Methods in Engineering*, vol. 42, pp. 1263-1278.

Zerroukat, M.; Djidjeli, K.; Charafi, A. (2000): Explicit and implicit meshless methods for linear advection-diffusion-type partial differential equations. *International Journal for Numerical Methods in Engineering*, vol. 48, pp. 19-35.

Zheng, R.; Phan-Thien, N.; Coleman, C. J. (1991): A boundary element approach for non-linear boundary-value problems. *Computational Mechanics*, vol. 8, pp. 71-86.

Zheng, R.; Phan-Thien, N. (1992): Transforming the domain integrals to the boundary using approximate particular solutions: a boundary element approach for non-linear problems. *Applied Numerical Mathematics*, vol. 10, pp. 435-445.